Polarimetric Radar Modeling of Mixtures of Precipitation Particles

J. Vivekanandan, Ravikumar Raghavan, *Member, IEEE,* and V. N. Bringi

Abstract— **With the recent advances of dual-polarized radar techniques in meteorology it is now possible to deduce precipitation microphysical characteristics in far more detail than possible with reflectivity measurements alone. Radar parameters such as differential reflectivity and differential phase between horizontal and vertical polarizations have been studied in detail as well as linear depolarization ratio, copolar correlation coefficient, and backscatter differential phase. While these parameters can be linked to certain microphysical properties of specific classes of precipitation such as raindrops or hail, very little study has been directed at the practically important cases of mixtures of different types of precipitation particles such as rain, hail, graupel, ice crystals, and snow. Each type can have different size, shape, orientation, and dielectric constant distributions. The treatment here is rigorous and is based on the Mueller matrix formulation. Radar parameters are derived from the averaged Mueller matrix computations. Careful consideration is given to the orientation and size distributions of the different particle types. After calculating single particle scattering characteristics, some simple two-component mixtures such as rain/hail and ice crystals/snow are considered. Finally, a 2D numerical cloud model is used to simulate the rain, hail/graupel, and snow fields of an evolving convective storm from which the radar parameters are derived for the initial, peak, and dissipating stages of the storm. Model computations are performed at C and S-band frequencies.**

I. Introduction

POLARIMETRIC radar techniques are finding a wide range of application in the remote sensing of storm microphysics. A number of research radars in the 3–35 GHz range have been modified for dual-polarization capability. See [1] for a review of many of these radar systems. While the earlier Canadian work by McCormick, Hendry and coworkers relied primarily on circular polarization techniques, more recent work has concentrated on linear horizontal (H) and vertical (V) polarizations. The radar parameters currently receiving a great deal of attention both theoretically and experimentally are differential reflectivity (Z_{DR}) [2] , linear depolarization ratio (LDR), specific differential phase (K_{DP}) [3], copolar correlation coefficient (ρ_{HV}) [4], and differential backscatter phase (δ) [5]–[7]. A coherent radar capable of switching the transmit polarization between H and V states and sequentially measuring the received copolar echo can measure all of the above parameters except LDR. Let (S_{HH}, S_{HV}, S_{VV}) be the complex backscatter amplitudes and let (f_{HH}, f_{VV}) be the complex forward-scatter amplitudes. By appropriate coherent processing of the backscatter samples the radar parameters can be derived and related to (S) and (f) as follows: reflectivity at H-polarization or $Z_H \propto < |S_{HH}|^2 >$, $Z_{DR} \propto < |S_{HH}|^2 > \div < |S_{VV}|^2 >$, $LDR \propto, < |S_{HV}|^2 > \div < |S_{HH}|^2 >$, $\rho_{HV} \propto |< S_{HH} S^*_{VV} >|$, $\delta \propto < arg(S_{HH} S^*_{VV}) >$ and $K_{DP} \propto < \mathrm{Re}(f_{HH} - f_{VV}) >$. The angle brackets denote ensemble averaging over particle sizes, dielectric constant and orientations. In rainfall, it is well known that Z_{DR} is a good estimator of mean oblateness while K_{DP} is a good estimator of rain rate.

Detection of mixed phase precipitation and quantification of the same is a complex problem compared to that of rain or ice phase alone. LDR signals ≥ -25 dB are observed in mixed-phase precipitation. Normally power in the cross-polarized channel is weak but it can be enhanced by the presence of a water coat on tumbling ice particles. Thus the utility of LDR may be restricted to the melting layer and wet growth regions. ρ_{HV} depends on a number of microphysical factors such as size, shape and differential phase shift upon backscattering (δ). δ depends on size of the nonspherical scatterer with respect to wavelength. Low values of ρ_{HV} may also be used to detect hail [4]. In mixed phase precipitation, Z and Z_{DR} are affected by both isotropic scatterers (tumbling hail, graupel) and anisotropic scatterers (raindrop, ice crystals). However, K_{DP} depends only on anisotropic scatterers. Thus it may be possible to estimate mixed phase precipitation particles by using Z, Z_{DR} and K_{DP}. The same technique may be extended for a precipitation media containing a mixture of pristine ice crystals (nonspherical scatterers) and aggregates (low density spheres).

In this paper, a generalized polarimetric radar model is used to consider mixed-phase precipitation and effects of larger radar elevation angles [8]. An outline of the generalized polarimetric model is given in Section II. Multiparameter radar parameters are derived from the averaged-Mueller matrix elements. The various assumptions relating to the input parameters such as particle shape, size, density and orientation for the different precipitation types considered in this study are described in Section III. The corresponding single-scatter radar observables are discussed for rain, hail, graupel, ice crystals, and snow. The radar modeling of precipitation comprising rain and ice (wet hail) and precipitation comprising pristine ice crystals (plates) and snow (aggregates) are dealt with in

Manuscript received March 26, 1993. This work was supported by the FAA under Contract DTFA01–90–Z-02005 and the National Science Foundation under Contract ATM-9214864. The work of R. Raghavan was also supported by NASA through USRA under Contract NAS8–37140. The National Center for Atmospheric Research is sponsored by the National Science Foundation.

J. Vivekanandandan is with the National Center for Atmospheric Research, Boulder, CO 80307.

R. Raghavan is with the USRA-NASA/Marshall Space Flight Center, ES42, Huntsville, AL 35812

V. N. Bringi is with the Department of Electrical Engineering, Colorado State University, Ft. Collins, CO 80523.

IEEE Log Number 9210724.

Section IV. Section IV also addresses the effects of large elevation angles on the radar signatures. To demonstrate the applicability of the above described modeling technique, realistic 2-dimensional (2D) cloud model microphysical outputs are used to drive the radar model. The 2D cloud model is initialized with sounding procured on June 28, 1989, during the North Dakota Thunderstorm project. Section V describes the resultant radar signatures of precipitation comprising rain, ice (hail and graupel), and snow. Finally, Section VI concludes with a summary of the results.

II. Radar Modeling Of Mixed Phase Precipitation

A detailed description of the radar model is given in [8]. The 2×2 backscatter matrix of rotationally symmetric targets is computed assuming an advantageous particle orientation via the T-matrix approach [9]. The technique proposed by [10] is then used to adapt the backscatter matrix for an arbitrary particle orientation. After the elements of the backscatter matrix are computed for an arbitrary particle orientation, the standard Stokes parameters are used to completely characterize the scattered field to yield the 4×4 Mueller matrix. The elements of the Mueller matrix are then averaged over the specified orientation distributions. A final Mueller matrix $\boldsymbol{S}$ representation is derived by integrating the individual Mueller matrices over the size distributions and over different hydrometeor types (rain, hail, snow and pristine ice crystals) that constitute mixed phase precipitation. The effects of larger elevation angles is also incorporated. Similarly, the forward scattering matrix and the corresponding extinction matrix $\boldsymbol{K}$ are computed.

The conventional radar parameters such as reflectivity at H-polarization (Z_H) differential reflectivity (Z_{DR}) and linear depolarization ratio (LDR) can be defined in terms of the elements of $\boldsymbol{S}$ as [8],

$$Z_H = \frac{2\pi\lambda^4}{|k|^2\pi^5}(S_{11} - S_{12} - S_{21} + S_{22}) \tag{1}$$

$$Z_{DR} = 10\log\left(\frac{S_{11} - S_{12} - S_{21} + S_{22}}{S_{11} + S_{12} + S_{21} + S_{22}}\right) \tag{2}$$

$$\mathrm{LDR} = 10\log\left(\frac{S_{11} - S_{12} + S_{21} - S_{22}}{S_{11} - S_{12} - S_{21} + S_{22}}\right) \tag{3}$$

where $k = (\epsilon_r - 1)/(\epsilon_r + 2), \epsilon_r$ being the particle dielectric constant. The copolar correlation coefficient ρ_{HV} and the backscatter differential phase δ between H and V polarized waves is given as

$$\rho_{HV} = \frac{2\pi\lambda^4}{|k|^2\pi^5}\frac{\left[(S_{33} + S_{44})^2 + (S_{43} - S_{34})^2\right]^{1/2}}{(Z_H Z_V)^{1/2}} \tag{4}$$

$$\delta = \arctan\left[\frac{S_{43} - S_{34}}{S_{33} + S_{44}}\right]. \tag{5}$$

The specific differential phase K_{DP} is defined as

$$K_{DP} = \frac{180}{\pi}\mathrm{K}_{34}. \tag{6}$$

The specific attenuation at H-polarization (A_H) (dB km^{-1}) can be expressed as follows:

$$A_H = -.4343(\mathrm{K}_{11} - \mathrm{K}_{21}). \tag{7}$$

III. Scattering Characteristics Of Single Particles at C-band

Electromagnetic scattering characteristics depend on the size, shape, dielectric constant, and orientation of the particles relative to the incident wave direction (elevation angle of incident beam). We consider only two shapes: oblate and conical. A variety of dielectric constants are considered to encompass low density to wet particles. The orientation is specified by the angles (θ, ϕ) of the particle symmetry axis relative to a XYZ system where the z-axis is along the local vertical direction. A two-dimensional orientation probability distribution is considered with $p(\theta, \phi) = p_1(\theta)p_2(\phi)$. The distribution $p_1(\theta)$ is modeled as Gaussian $(\bar{\theta}, \sigma)$ while the distribution $p_2(\phi)$ is uniform in the interval $(0, 2\pi)$. We refer to [8] for more details. For single particles considered in this section, the Gaussian distribution is chosen with very small $\sigma = 0.1°$ and $\bar{\theta}$ = 0 or 90°. The equivolumic spherical diameter is D which is also referred to as particle size. We consider five particle types, these being raindrops, hail, graupel, ice crystals, and snow.

The symmetry axis of raindrops, graupel, plates, and snow particles is aligned along the vertical direction ($\bar{\theta} = 0°$); this orientation which has the longer dimension along the horizontal direction is often referred to as H-orientation. For sizes small relative to wavelength, this orientation gives positive Z_{DR}. For the oblate hail particles, the symmetry axis is randomly oriented in the horizontal or XY plane ($\bar{\theta} = 90°$, random ϕ). This orientation gives negative Z_{DR} for small sizes since the longer dimension is along the vertical direction (also termed as the V-orientation). Experimental observations of Z_{DR} in hail regions often show negative values [4], [11], and [12] which is the reason we also have chosen this particular orientation. Table I gives an overview of the main assumptions used for the different particle types. In this section only individual particle sizes are considered. The narrow σ of 0.1° is used in the Gaussian distribution to simulate preferred orientation.

Fig. 1 shows model calculation for H-oriented raindrops at zero elevation angle. Since Z_H and K_{DP} depend on particle concentration we assume here a concentration of 1 per m^{-3}. Both Z_{DR} and δ display resonance effects in the size range 5–7 mm [15]. Such effects have been noted experimentally at C-band [5]. The increase in Z_H with size is according to Rayleigh scattering, i.e., proportional to D^6. The increase in Z_{DR} and K_{DP} with size is due to increasing oblateness of the raindrops (axis ratio decreases from unity). While Z_{DR} can be related to the mean axis ratio of the drops and hence to mean drop size, K_{DP} can be related to rain water content or rain rate. The parameter δ is a good indicator of Mie scattering for oblate particles. For raindrops at C-band, δ deviates from zero at around 4 mm, and shows a sharp transition from negative to positive values near 5.5 mm. This variability in δ causes the copolar correlation coefficient ρ_{HV} (for an ensemble of drop sizes) to decrease from unity. Observations of K_{DP} and δ at C-band are given in [5].

Fig. 2 shows the radar parameters for dry, spongy, and wet hail particles in the size range 5–40 mm. We emphasize the orientation of the oblate spheroid which has its symmetry axis

TABLE I
MICROPHYSICAL CHARACTERISTICS OF HYDROMETERS

Type	Size	Shape	Orientation	ϵ (Dielectric Constant)
Raindrops	Exponential DSD 0.1-8mm	oblate equilibrium $\frac{a}{b}$ *vs* D	$\bar{\theta} = 0°$, σ	water at 10°C $\epsilon = 70.9 + j29.4$
Hail	Cheng & English [25] DSD 5-40mm	oblate $\frac{a}{b} = 0.75$	$\bar{\theta} = 90°$, σ	(i) wet - water at 0°C (ii) spongy - VI= 0.6; VW=0.4 Longtin et al. (1987) [13] $\epsilon = 22.66 + j11.41$
Graupel	Exponential DSD 0.1-5mm	conical, oblate bottom, apex pointing up [17]	$\bar{\theta} = 0°$, σ	dry; $VI = 0.5$; $\epsilon_r = 1.97 + j0.271 \times 10^{-3}$ spongy; $VI = 0.6$; $\epsilon_r = 22.66 + j11.41$ wet; $\epsilon = 65.47 + j37.02$
Ice Crystals/ Plates	Exponential DSD 0.1-5mm	oblate $\frac{a}{b} = 0.2$	$\bar{\theta} = 0°$, σ	ice $\rho = .9gm\ cm^{-3}$
Snow	Exponential DSD 2-20mm	oblate $\frac{a}{b} = 0.8$	$\bar{\theta} = 0°$, σ	(i)$\rho = 0.2,\ 0.5,\ 0.8\ gm\ cm^{-3}$; VI = ρ, VW = 0 $\rho = 0.2$, $\epsilon = 1.33 + j8.09 \times 10^{-5}$ $\rho = 0.5$, $\epsilon = 1.97 + j2.71 \times 10^{-4}$ $\rho = 0.8$, $\epsilon = 2.78 + j6.12 \times 10^{-4}$ (ii) spongy, $VI = 0.6, VW = 0.4$

Note: DSD = drop size distribution. $\frac{a}{b}$ = axis ratio of oblate particle, ratio of minor to major axis; for raindrops refer to Green [14]. ρ = density of particle. VI = volume fraction of ice; VW = volume fraction of water. Two-dimensional orientation distribution $p(\theta, \phi) = p_1(\theta)p_2(\phi)$, where $p_1(\theta)$ is Gaussian $\bar{\theta}$ = mean; σ = standard deviation; $p_2(\phi)$ is uniform $(0, 2\pi)$. In Figs. 1–4: $\sigma = 0.1°$ is used for single particles. In Figs. 5, 6: Raindrops $\sigma = 5°$, hail $\sigma = 1°$. In Figs. 7, 8: Plates $\sigma = 0.5°$, snow $\sigma = 30°$. In Figs. 9–11: Raindrops $\sigma = 5°$, wet hail/spongy graupel/dry snow $\sigma = 45°$.

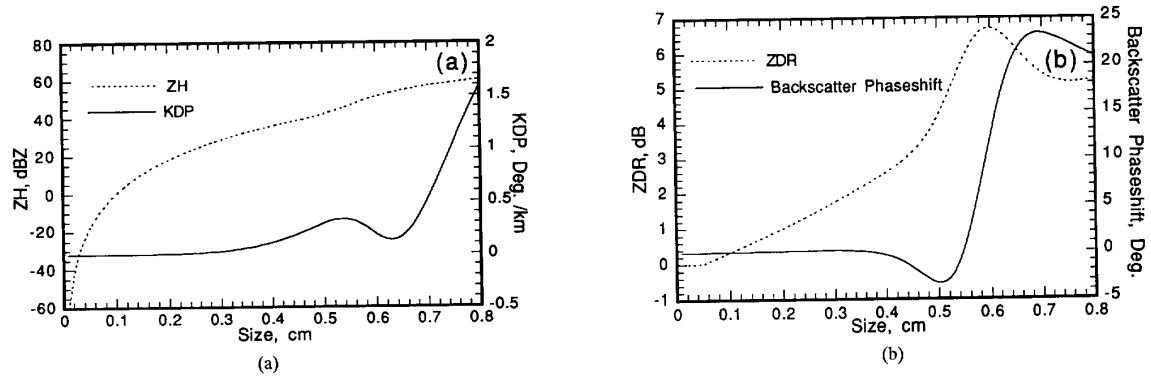

Fig. 1. Single scattering characteristics of raindrops (a) reflectivity (Z_H), propagation phaseshift (K_{DP}) and (b) differential reflectivity Z_{DR}, phaseshift upon backscatter δ versus equivolumic spherical diameter of raindrops at C-band. Axis ratios based on Green [14].

in the horizontal plane ($\bar{\theta} = 90°$, random ϕ). Because of random ϕ, the principal cross section of the spheroid appears (at zero elevation angle) to change from the extremes of circular and elliptical shapes. This averaging is inherent in the calculations shown in Fig. 2. Strong resonant-type behavior is reflected in all the radar parameters. The spongy and wet hail curves are in close agreement whereas the dry hail curves are significantly different. For sizes $\leq$ 15 mm, the V-orientation of the particles gives negative Z_{DR}, K_{DP} and δ. While Z_{DR} is mainly negative for spongy/wet hail, it reverses the sign for dry hail at 27 mm as noted previously [16]. K_{DP} also reverses the sign for dry hail at 27 mm. It is interesting to note that while Z_{DR} is negative for spongy/wet hail over the whole size range, the K_{DP} is positive and increases with size for D $\geq$ 17mm. Thus, the backscatter and forward-scatter properties are vastly different. The backscatter differential phase δ shows strong resonant behavior previously noted at S-band [4]. Techniques for estimating δ are discussed in [6] and [7] using radar data at C and S-bands. The copolar correlation coefficient ρ_{HV} is shown in Fig. 2(e). For a given size, the decrease from unity is due to the random ϕ of the symmetry axis alluded to earlier. For dry hail, a local dip in ρ_{HV} is seen at 27 mm, which is well-correlated with the sign reversal in Z_{DR} (see Fig. 2(c)), K_{DP} (Fig. 2(b)) and δ (Fig. 2(d)). For spongy/wet hail, a dip in ρ_{HV} occurs at 30 mm which is correlated with a local Z_{DR} minimum (Fig. 2(c)). It is important to note that

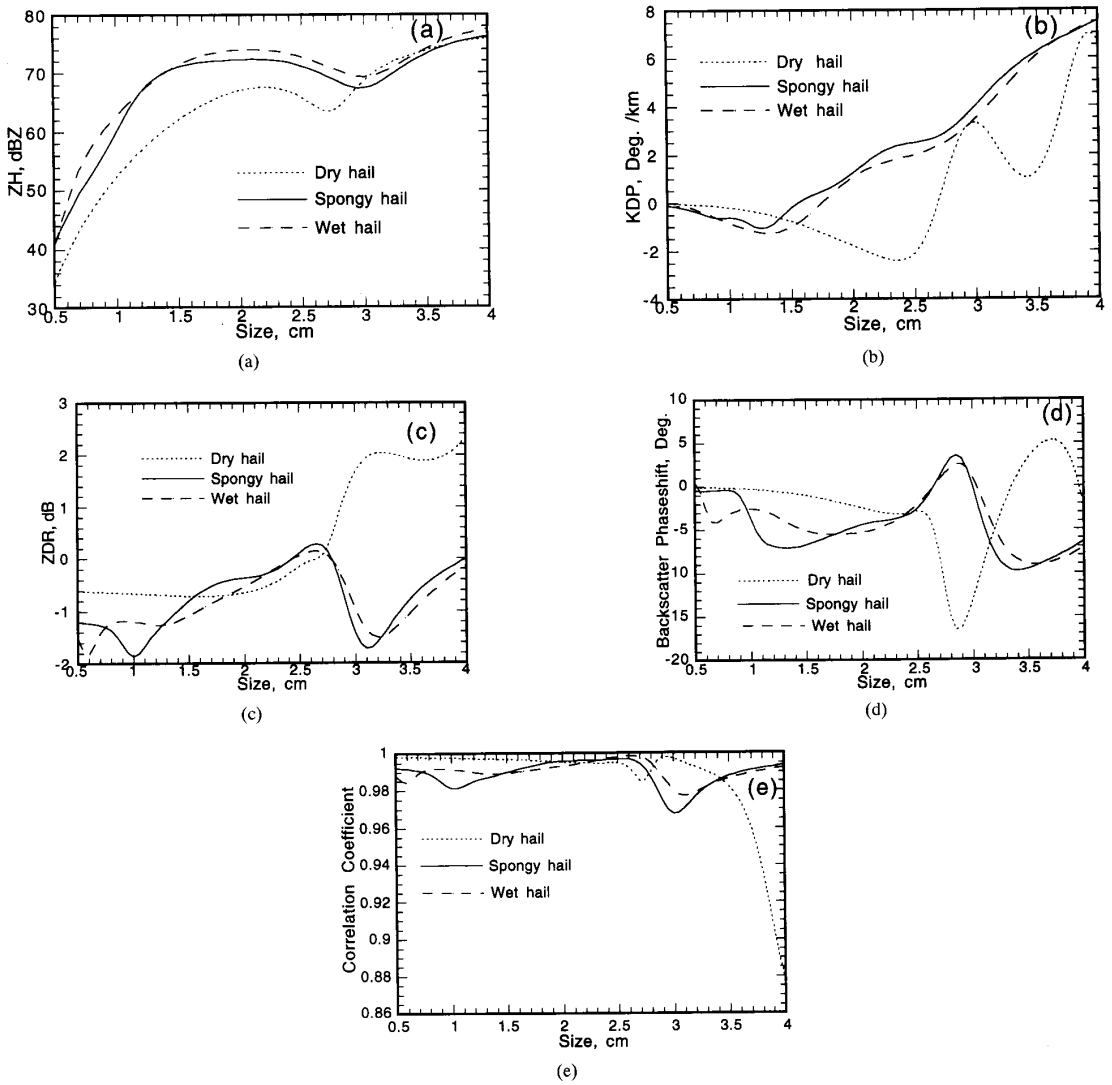

Fig. 2. Single scattering characteristics of hailstones of axis ratio 0.75 (a) reflectivity (Z_H), (b) propagation phaseshift (K_{DP}), (c) Z_{DR}, (d) backscatter phaseshift (δ), (e) correlation ρ_{HV} versus equivolumic spherical diameter at C-band. Modeled are dry, spongy and wet hail. Hailstones have their minor axis randomly oriented in the horizontal plane.

when integrating over a size distribution the ρ_{HV} will decrease further due to variable δ versus size [4]. It has been suggested that low ρ_{HV} can be used to infer hail in convective storms [4].

Fig. 3 shows model calculations for plates and graupel (wet/spongy/dry). Graupel are modeled as conical in shape with an oblate bottom and apex pointing vertically upward. The shape is such that the longest dimension is along the horizontal direction (H-orientation) [17], which gives positive Z_{DR} as shown in Fig. 3(c). Plates give the highest Z_{DR} because of their low axis ratio. Z_{DR} does not change with size since the shapes are fixed and the particle size is small compared to wavelength (note $\delta \approx 0^o$). Experimental radar observations indicate that positive Z_{DR} in winter storms can be correlated with plate-type crystals [18]–[20]. Oriented plate-type crystals can also give rise to positive K_{DP} (Fig. 3(b)); see also the experimental radar observations reported in [21]. The graupel calculations show close similarity between spongy/wet cases. Dry graupel has also low Z_{DR} because of low dielectric constant. Conical graupel has been observed in one case using aircraft imaging probes [22] with corresponding Z_{DR} observed by radar in the range 0.4–2.0 dB. In convective storms it is likely that graupel particles will tumble or oscillate and this will reduce Z_{DR} and K_{DP} to near zero.

Fig. 4 shows model calculations for H-oriented oblate snow particles with varying densities of 0.2, 0.5, and 0.8 gm cm^{-3} as well as a spongy case. The various curves show the dependence of radar parameters with size and dielectric constant. While it is not realistic to expect snow particles to be preferentially oriented, the curves give a general idea about the expected minimum values given that snow particles are

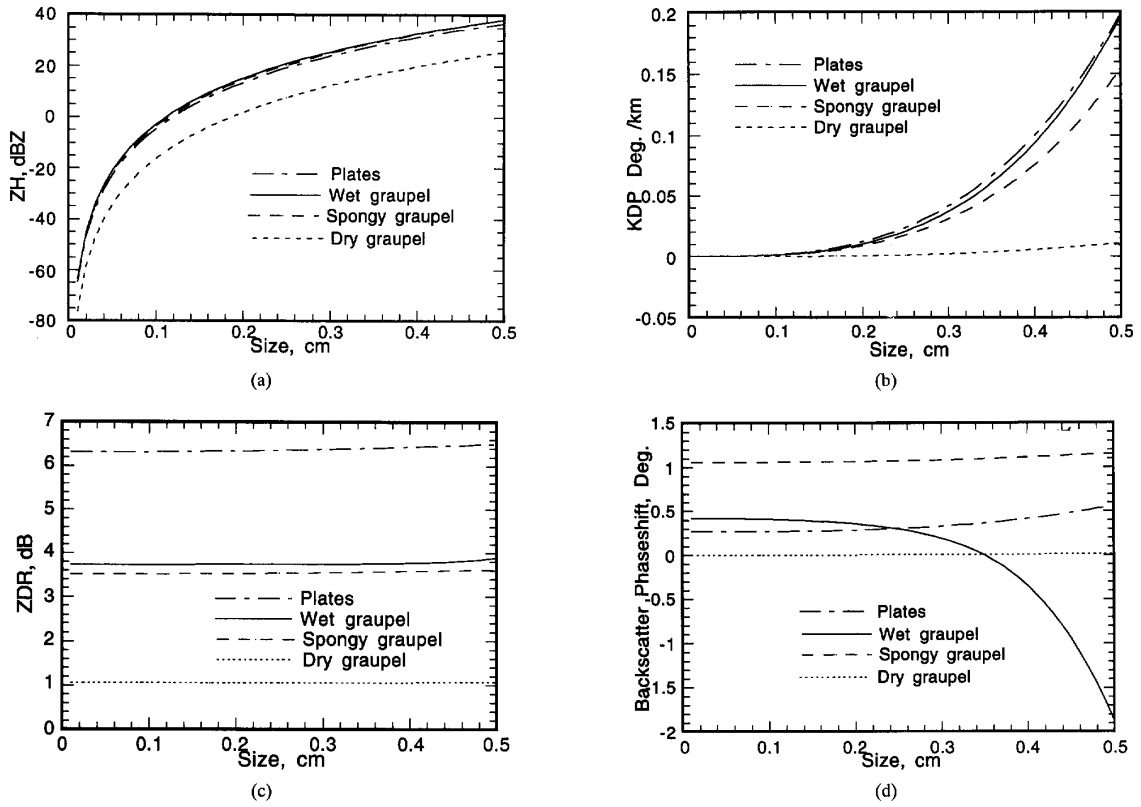

Fig. 3. Single scattering characteristics of conical graupel and oblate ice crystals (axis ratio=0.2) (a)Z_H, (b) K_{DP}, (c) Z_{DR}, (d) δ versus equivolumic spherical diameter at C-band. Modeled are dry, spongy and wet graupel.

often irregular in shape and tumble or gyrate when falling. However, in the stratiform melting layer a peak Z_{DR} is often noticed at the base of the "bright band" which corresponds to very wet snow particles just before they collapse into tiny raindrops. Also, δ can be inferred in this region whenever the snow particles are large. A good discussion of radar measured Z_{DR} and δ within the "bright band" is given in [7]. Fig. 4(c) shows that Z_{DR} is very sensitive to dielectric constant. Also, resonance effects are noticed for the spongy snow case which can also be used for wet snow, i.e., to infer melting snow processes within the "bright band." From Fig. 4(d) one can infer that δ is not important unless the snow is wet. The measurement of δ at the base of the melting layer can be indicative of maximum snow size [7].

IV. Mixed Phase Precipitation

A. Rain and Wet Hail at S-Band

Precipitation below the melting level consists of a varying mixture of hydrometeors of diverse shape, size, and thermodynamic phase. Below the melting level in convective storms it is common to observe mixed-phase precipitation comprising rain and hail. In this section, the effect of a mixture of rain and wet hail on the multiparameter radar observables is considered [4]. A constant rain rate of 75 mm\h^{-1} and a Marshall-Palmer size exponential distribution [23] for the raindrops is assumed. The orientation distribution is modeled as a Gaussian with the raindrop minor axis oriented along the vertical. The hailstones are assumed to have a fixed axis ratio of 0.75 [24] and are modeled as oblate spheroids oriented with their minor axes in the horizontal plane. The hailstones are assumed to follow the Cheng and English size distribution [25] of the form

$$N(D) = N_o\, e^{-\Lambda D} \tag{8}$$

$$N_o = 115\ \Lambda^{3.63} \tag{9}$$

where N_o is in units of mm^{-1} m^{-3}, Λ is in mm^{-1} and D is in mm. This distribution allows the convenience of using a single parameter to describe the hail precipitation or hail fall rate R_h (mm\h^{-1}) that is related to Λ by [26].

$$\Lambda = \ln(88/R_h)\ /\ 3.45 \tag{10}$$

The hail rate R_h in this study was varied from 0 to 40 mm\h^{-1}. The minimum and maximum equivalent diameters for the hailstones are taken as 5 and 40 mm, respectively. It has been shown [27] that integral parameters such as reflectivity are insensitive to changes in the product ΛD_{max} for values of $\Lambda D_{max} > 5$, thus justifying the choice of large D_{max}. See Table I for details on rain and hail particles.

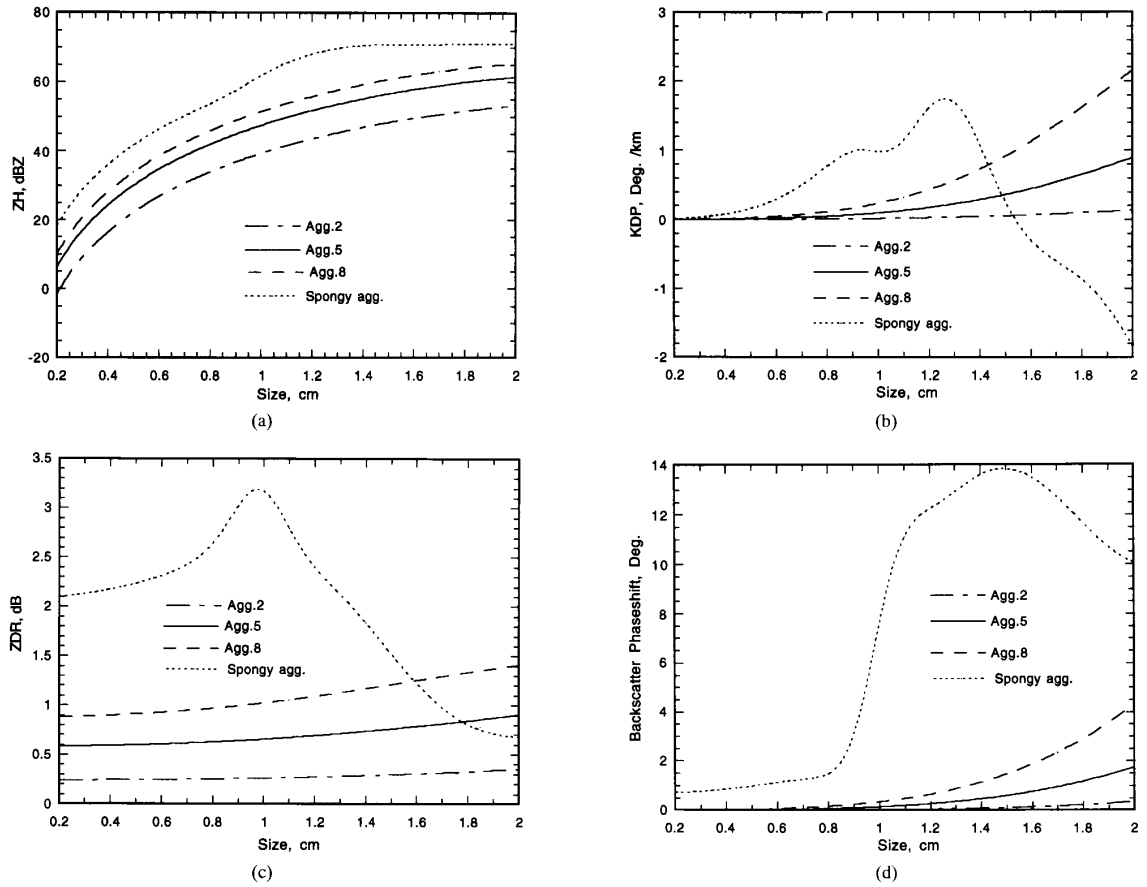

Fig. 4. Single scattering characteristics of aggregates (axis ratio=0.8) of densities 0.2, 0.5, and 0.8 g\cm^{-3} (a) Z_H, (b) K_{DP}, (c) Z_{DR}, (d) δ versus equivolumic spherical diameter at C-band. Also modeled are spongy aggregates with 40% water fraction.

Fig. 5 shows the radar observables plotted versus hail rate R_h for fixed rain rate of 75 mm\h^{-1}. Z_H increases from 53 to 71 dBZ due to the increasing hail in the mixture. Z_{DR} decreases with increasing R_h and the dominance of the hailstones in the mixture is also indicated by the flat part of the Z_{DR} profile in Fig. 5(b). In Fig. 5(c), ρ_{HV} decreases with increasing R_h, albeit the decrease with R_h is not monotonic. The ρ_{HV} profile exhibits a minimum. The minimum value of ρ_{HV} is not strongly dependent on the amount of rain in the mixture; it is more dependent on the hail rate at the point where the minimum occurs. The minimum may be explained by the increasing contribution to ρ_{HV} from hailstones and occurs at a point where rain and hail reflectivities are comparable. Beyond the minimum, hailstones dominate and ρ_{HV} increases. Figs. 5(d), (e) show profiles of K_{DP} and δ with varying R_h. The K_{DP} profile is sensitive only to the raindrops and is affected very little by the addition of hailstones. This is due to the smaller dielectric constant and tumbling of the hailstones compared with that of raindrops. The δ profile varies by $\sim 4°$ with increasing R_h. It is noteworthy that the effective width of δ, and hence the reduction in ρ_{HV}, is influenced by the hail size distribution.

Polarimetric observables also depend upon the elevation angle of the incident radar beam. Fig. 6 shows the elevation angle dependence of the radar observables for a fixed hail rate of 5 mm\h^{-1}. Most of the observables except LDR asymptotically approach the values exhibited by spherical scatterers at an elevation angle of 90°. LDR increases with elevation angle due to an apparent increase in shape dispersion. It is interesting to note that the polarimetric radar observables are relatively insensitive to elevation angles up to 20° and hence elevation angle effects up to 20° on the observables can be ignored.

B. Pristine Ice Crystals (Plates) and Aggregates at C-Band

Mixed phase precipitation is also prevalent in winter storms where pristine ice crystals such as plates and needles aggregate to form snow particles. The effect of the mixture of ice crystals and aggregates on the multiparameter radar observables is considered here. The ice crystals (plates) are assumed to have a fixed axis ratio of 0.2 and are modeled as oblate spheroids. The ice crystals are assumed to follow an exponential size distribution of the form

$$N(D) = N_o\, e^{-(3.67\ D/D_o)} \tag{11}$$

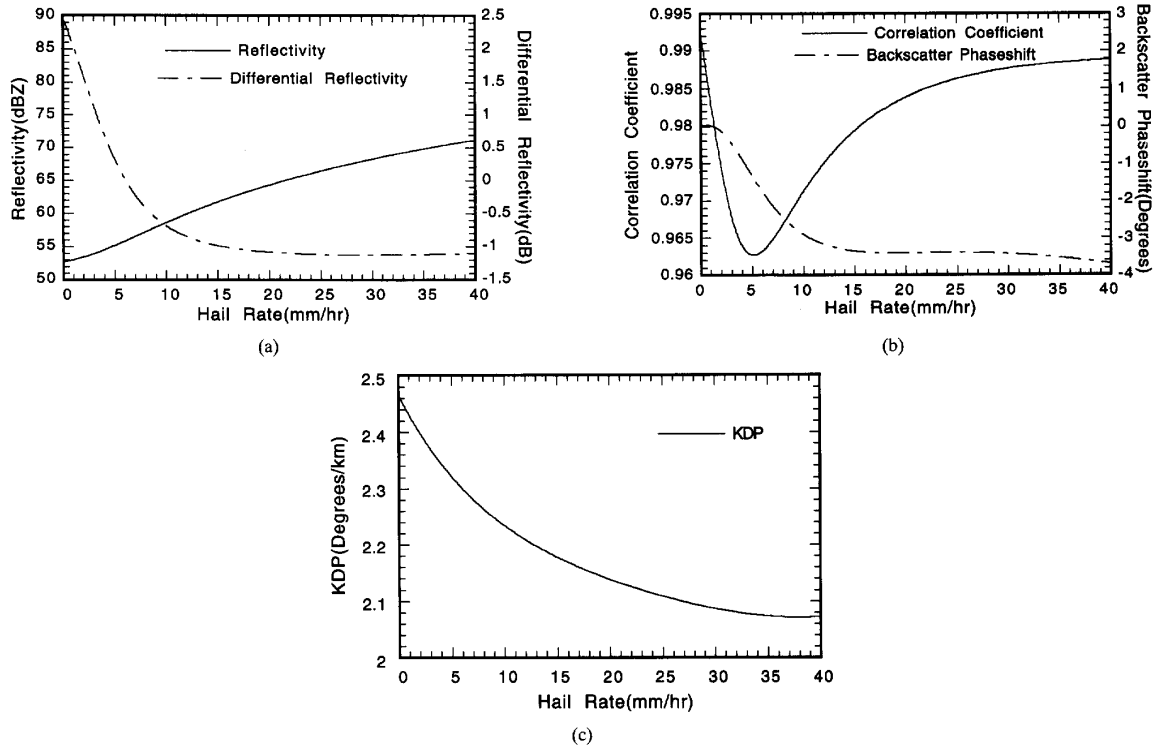

Fig. 5. Profile of (a) reflectivity (Z_H), differential reflectivity (Z_{DR}) and (b) correlation (ρ_{HV}), (c) K_{DP} against hail rate for precipitation comprising rain and wet hail at S-band. The rain rate is assumed constant at 75 $mm\ h^{-1}$. Marshall-Palmer DSD (1948) is assumed for rain while hail follows the Cheng and English DSD [25].

where $N_o = 124.54\ mm^{-1}\ m^{-3}$, $D_o = 1.0\ mm$ are chosen such that the reflectivity of the ice crystals is constant at 10 dBZ in the mixture. The orientation distribution is modeled as a Gaussian with the plate's minor axis oriented along the vertical. The aggregates are assumed to have a bulk density of 0.2 g\cm^{-3} and a fixed axis ratio of 0.8. They are modeled as oblate spheroids oriented with their major axis in the horizontal plane. The aggregates are assumed to follow an exponential size distribution of the form in (12) where the parameters N_o and D_o are chosen such that the aggregate reflectivity in the mixture varies between -5 and 25 dBZ. The orientation distribution is modeled as a Gaussian with zero mean and $\sigma = 30°$ to simulate the fall-mode behavior (tumbling) of aggregates. Details about size and composition of these two hydrometeor types are given in Table I.

Fig. 7 shows the profiles of the radar observables plotted versus varying aggregate reflectivity (Z_{AGG}) for a fixed plate reflectivity of 10 dBZ. Z_{AGG} is varied from -5 to 25 dBZ. The ρ_{HV} profile decreases with increasing Z_{AGG} and exhibits a minimum where reflectivities due to plates and aggregates are comparable. Beyond the ρ_{HV} minimum, reflectivity due to aggregates dominate. The Z_{DR} profile also decreases with increase in Z_{AGG}. The initial high values of Z_{DR} are due to the dominance of the plates in the mixture, while the dominance of the tumbling aggregates in the mixture is indicated by the low values of Z_{DR}. The LDR profile increases as Z_{AGG} increases because the tumbling aggregates cause significant depolarization as compared to the highly aligned plates. The small values of δ in Fig. 7(a) show the Rayleigh scattering effects. K_{DP} is sensitive only to the oriented plates and is independent of change in aggregate reflectivities. It is known that highly oriented plates contribute significantly to K_{DP} [21]. A_H values increase as the total mass of the mixture medium increases, but is negligible.

Fig. 8 shows the elevation angle dependence of the radar observables for a fixed aggregate reflectivity of 10 dBZ. Since both plates and aggregates were modeled as oblate spheroids, the radar observables tend to the values exhibited by spherical scatterers as the elevation angle increases to 90°. It is evident from Fig. 8 that the elevation angle effects on the radar observables can again be ignored for angles less than 20°.

V. Radar Modeling Of Precipitation Comprising Rain, Hail/Graupel, And Snow At C-band

In the study that follows a 2D cloud model was used to initialize the radar model. The cloud model provides vertical cross section ($x - z$) behavior versus time, of the cloud water, cloud ice, rain, hail/graupel and snow. A uniform grid spacing of 200 m was used, with an extent of 20 kms in both the x and z directions. The cloud model was initialized with sounding data procured on June 28, 1989 during the North Dakota Thunderstorm project. The model was run for a duration of 477 time steps, each step representing one minute of cloud evolution. A good description of the cloud model can be found in [28].

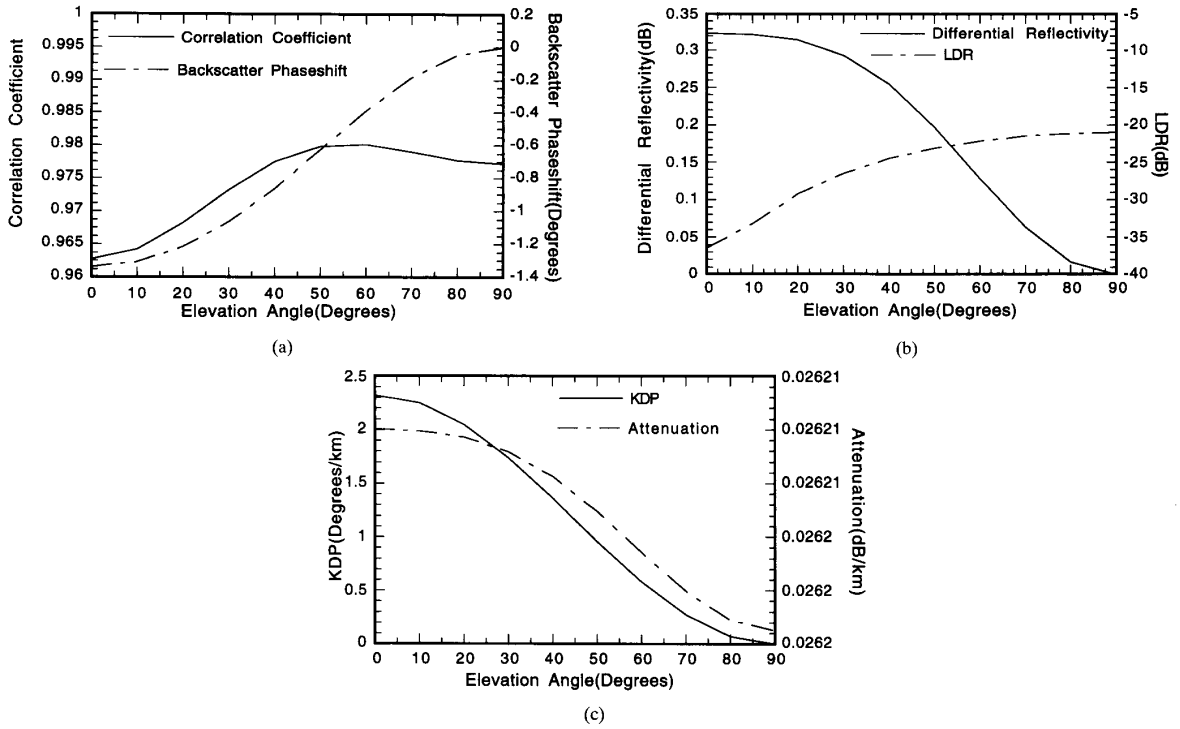

Fig. 6. Elevation angle dependence of the polarimetric radar observables at S-band. The precipitation medium comprises rain and wet hail. The rain rate is assumed constant at 75 $mm\ h^{-1}$. The hail rate is fixed at 5 $mm\ h^{-1}$. Marshall–Palmer DSD [23] is assumed for rain while hail follows the Cheng and English DSD [25].

This study considers only three time steps at 15 minute intervals, viz., 270, 285, and 300 minutes into the simulation. Time step 285 represents peak activity in the simulation of the storm event. For the purpose of radar modeling only rain, hail/graupel, and snow are considered. Since the bulk water 2D cloud model produces only mixing ratios, it is necessary to introduce assumptions regarding the drop size distributions (DSD) for each hydrometeor type in order to perform modeling computations to calculate the radar observables. The cloud model treats hail/graupel as one category and produces one mixing ratio. We assume that the size range 0–5 mm is graupel and 5–40 mm is hail, see Table I. The mixing ratios in units of $g\ g_{air}^{-1}$ were converted to individual mass contents of $g\ m_{air}^{-3}$ using Poisson's equation for adiabatic processes and the gas law [29].

An exponential size distribution of the form

$$N(D) = N_o\ e^{-\Lambda D} \tag{12}$$

was used for the rain, hail/graupel, and snow categories. This form of the DSD was chosen for reasons of simplicity, since the moments can be expressed in a compact closed form. The slope Λ of the DSD can be calculated from the closed form expression for the mass content M as

$$M = \pi\ \rho\ N_o\ /\ 1000\ \Lambda^4 \tag{13}$$

where M is the mass content in $g\ m^{-3}$, ρ is the assumed bulk density in $g\ cm^{-3}$, N_o is in units of $mm^{-1}\ m^{-3}$ and Λ is in units of mm^{-1}. The assumptions regarding particle size, shape, and composition are discussed in Table I.

The values assumed to characterize the exponential DSD for each category is as follows. For raindrops, $N_o = 8000\ mm^{-1}\ m^{-3}$ with $\rho = 1.0\ g\ cm^{-3}$. The hailstones were assumed to have a bulk density $\rho = 0.9\ g\ cm^{-3}$ and N_o was set to 8000\ $mm^{-1}\ m^{-3}$. $N_o = 8000\ mm^{-1}\ m^{-3}$ for graupel and ρ was set to 0.5 $g\ cm^{-3}$. A $N_o = 4000\ mm^{-1}\ m^{-3}$ and $\rho = 0.2\ g\ cm^{-3}$ was associated with snow. The mass contents M for eahch time step considered was provided through mixing ratios for each category by the cloud model. Λ was then computed using (14). At each time step and every grid point (grid spacing was 200 m), these distribution parameters were used to compute the vertical profiles of the size spectrum integrated scattering and extinction coefficients as well as the Mueller matrix. The multiparameter radar observables were then computed using the procedure outlined in Section II. A major advantage of using the output of a cloud model as input to a radar model is that it allows one to model regions of coexisting species, such as those considered in this study. A discussion of the modeling results obtained by coupling the radar model to the cloud model for the three time steps (270, 285, and 300) follows.

A. Time Step 270 in the Simulation

Figs. 9(a)–(c) show color profiles of mass content in the $x - z$ plane for rain (M_r), hail/graupel (M_h), and snow (M_s),

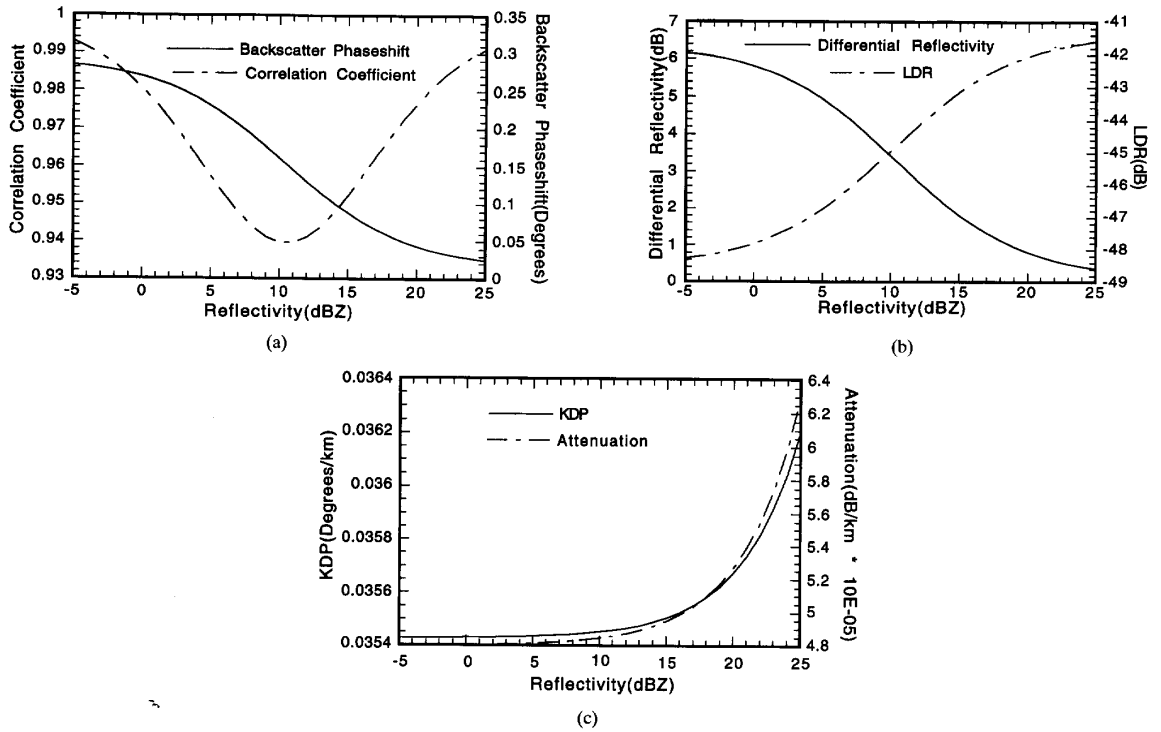

Fig. 7. Profiles of polarimetric radar observables against aggregate reflectivity (Z_{AGG}) for precipitation comprising ice crystals and aggregates at C-band. The reflectivity of the ice crystals is assumed constant at 10 dBZ. Exponential DSD is assumed for ice crystals and aggregates.

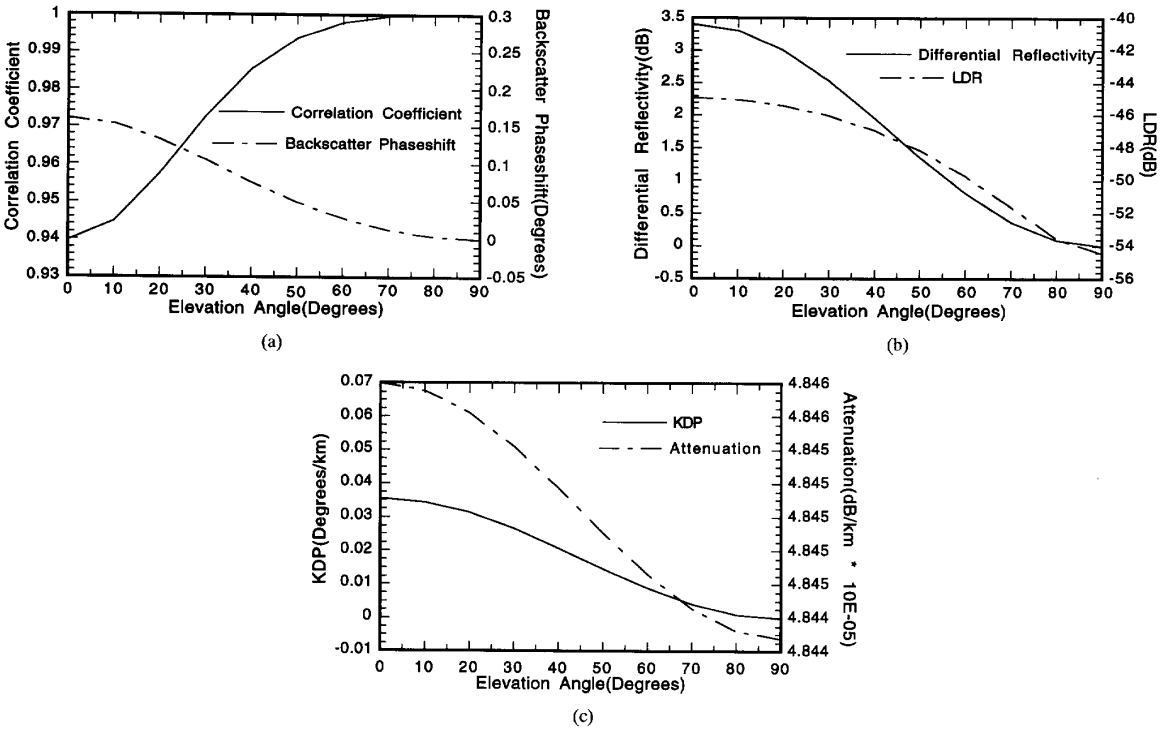

Fig. 8. Elevation angle dependence of the polarimetric radar observables at C-band. The precipitation medium comprises ice crystals and aggregates. The reflectivity of the ice crystals is assumed constant at 10 dBZ. The aggregate reflectivity Z_{AGG} is fixed at 10 dBZ. Exponential DSD is assumed for ice crystals and aggregates.

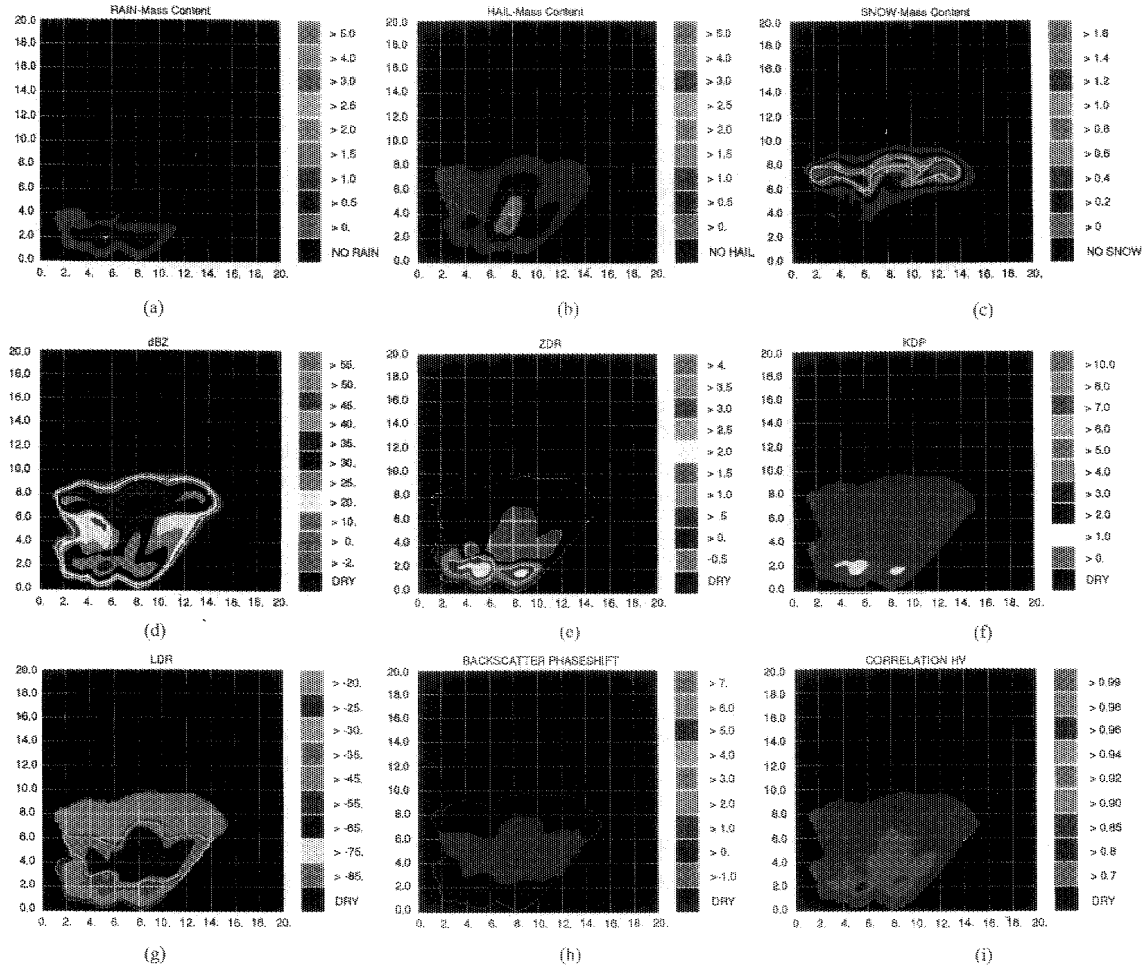

Fig. 9. $x - z$ contours of (a) rain mass content, (b) hail mass content, (c) snow mass content, (d) Z_H, (e) Z_{DR}, (f) K_{DP}, (g) LDR, (h) δ, (i) ρ_{HV} at time step 270. The mass contents are obtained from the 2D SDSM&T cloud model and the polarimetric observables obtained from the radar model which is coupled to the 2D cloud model. Modeled are raindrops, wet hail, spongy graupel, and dry snow at C-band.

respectively. In Fig. 9(a) the peak value of M_r is 1.55 $g\ m^{-3}$. The peak value of M_h in Fig. 9(b) is 2.23 $g\ m^{-3}$ while the peak value of M_s is 1.64 $g\ m^{-3}$ in Fig. 9(c). From Figs. 9(b) and (c) it is evident that there is significant ice phase precipitation present above the melting level ($\sim$ 4 km in North Dakota). Figs. 9(d)–(i) show color profiles of the computed multiparameter radar observables. In Fig. 9(d) it is seen that reflectivity (Z_H) values greater than 40 dBZ are coincident with the rain below 3 km in z and with the snow aloft. The hail shaft between 6 to 9 kms in x exhibits Z_H values greater than 35 dBZ. Z_{DR} in Fig. 9(e) has a peak value of 2.48 dB and is colocated with the peak in M_r. Below the melting level Z_{DR} values exceed 1.5 dB reflecting the presence of rain as compared to ice particles. The dominance of ice particles aloft is indicated by the low values of Z_{DR}. A region of negative Z_{DR} aloft, indicates the presence of tumbling hailstones. LDR values are low below 2 km in z due to the highly oriented raindrops. A broad bright band in LDR is seen around the melting level. This increase in LDR is due to the presence of tumbling hailstones and graupel in this region. Specific differential phase (K_{DP}) values are greater than $1^\circ km^{-1}$ in the rain medium and negligible aloft. This is as expected, since K_{DP} is sensitive only to raindrops and is almost transparent to the "quasispherical" ice as seen earlier in Section IV. Phase shift upon backscatter (δ) is very small at this time step. In Fig. 9(i) the copolar correlation coefficient (ρ_{HV}) decreases to 0.96 below the melting level. This decrease is likely due to the mixture of hydrometeor types (rain and hail/graupel) present at these levels as well as the δ effects due to large raindrops. Above the melting level ρ_{HV} values are > 0.98 indicating the presence of hydrometeors similar in composition. Attenuation values are very low at this time step indicating very low concentrations of water content even below the melting level.

B. Time Step 285 in the Simulation

Figs. 10(a)–(c) show color profiles of mass contents M_r, M_h, and M_s, respectively. In Fig. 10(a) M_r values exceed

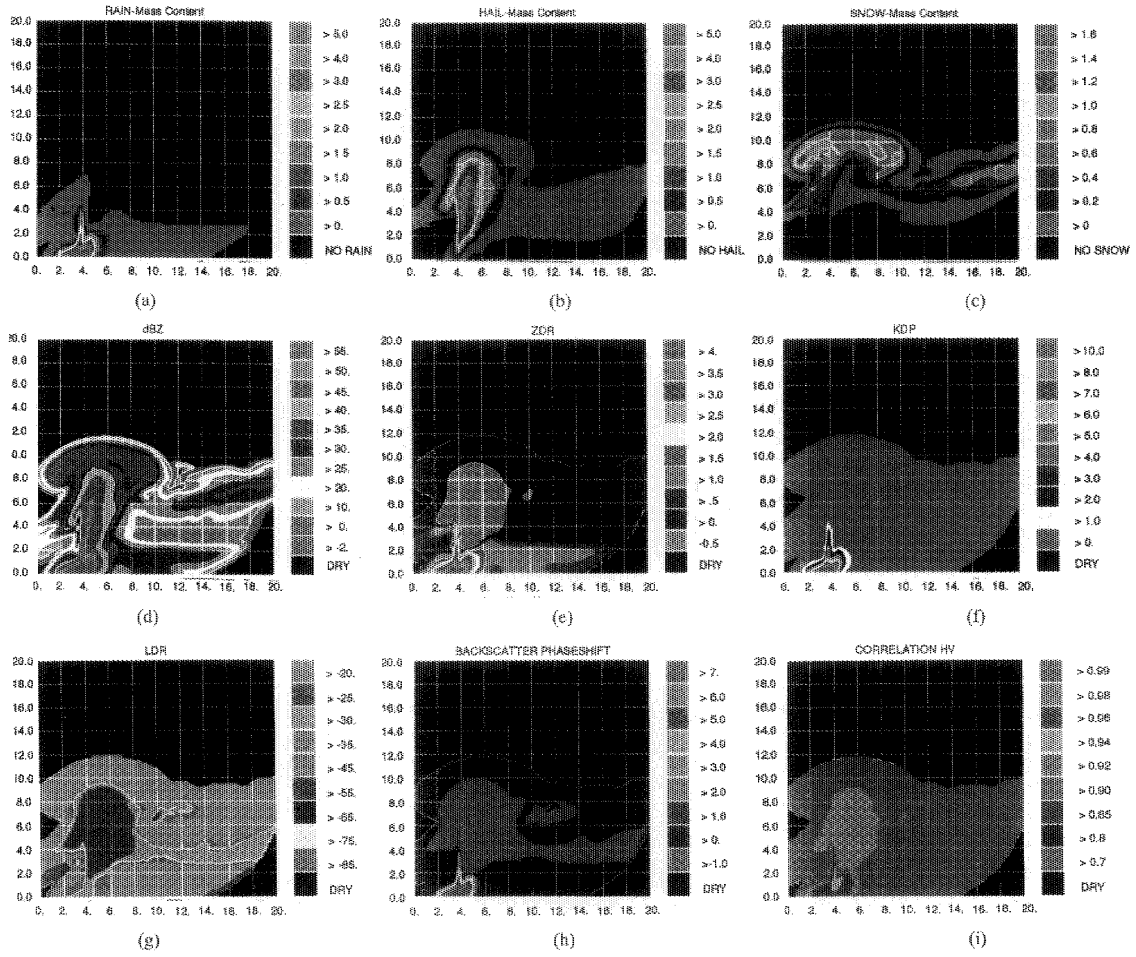

Fig. 10. Same as Fig. 9, except at time step 285.

6 $g\ m^{-3}$ near the surface and correspondingly one can infer intense rain rates at the surface. There is also an updraft of $\sim$ 24 $m\ s^{-1}$ which is carrying the raindrops to nearly 4 km in z. M_h values in Fig. 10(b) exceed 4 $g\ m^{-3}$ above the melting level indicating a large concentration of ice particles. Also evident at this time step is the descent of the hail shaft to the surface, although the concentration of ice particles is not large near the surface. M_s values in Fig. 10(c) are less than 1.32 $g\ m^{-3}$. Figs. 10(d)–(i) show color profiles of the radar observables. In Fig. 10(d), Z_H values exceed 55 dBZ below 2 km in z indicating intense rain. Z_H values greater than 45 dBZ are colocated with the hail shaft. Aloft, Z_H due to snow exceeds 35 dBZ. Z_{DR} values in Fig. 10(e) exceed 4 dB below 1 km in z over a 1–km range indicating the presence of large oblate particles. A region of negative Z_{DR} is seen aloft indicating the presence of tumbling hailstones falling with their minor axes in the horizontal plane. The narrow positive Z_{DR} column extending to the melting level is colocated with the updraft and verifies the presence of raindrops being carried aloft by the updraft. Such columns have been frequently observed before [28]. Z_{DR} values in excess of 1 dB around 8 to 12 km in x and below 2 km in z is indicative of precipitation comprising raindrops only. LDR values in Fig. 10(g) are very small below 3 km in z and above 9 km in z. A region of values $\geq$ -25 dB is seen extending above the melting level indicating the presence of tumbling hailstones as is also evident in the profile of M_h and Z_{DR}. K_{DP} values greater than $10^{\circ}km^{-1}$ are seen near the surface in Fig. 10(f). The narrow column of raindrops being supported by the updraft is evident in this figure. Elsewhere, K_{DP} values are $\sim$ $0^{\circ}km^{-1}$ indicating precipitation comprising mostly ice particles. Fig. 10(h) shows δ values exceeding 7° near the surface. The relatively high values of δ below the melting level is due to Mie effects caused by the larger sized raindrops. The effect of δ on ρ_{HV} is seen in Fig. 10(i), where ρ_{HV} decreases to 0.94 near the surface. The decrease in ρ_{HV} aloft is due to precipitation comprising different types of hydrometeors in addition to the δ effects. Elsewhere, ρ_{HV} = 0.98 indicating precipitation comprising similar type particles. Attenuation values are greater than 0.5 dB km^{-1} near the surface due to a larger rain mass content.

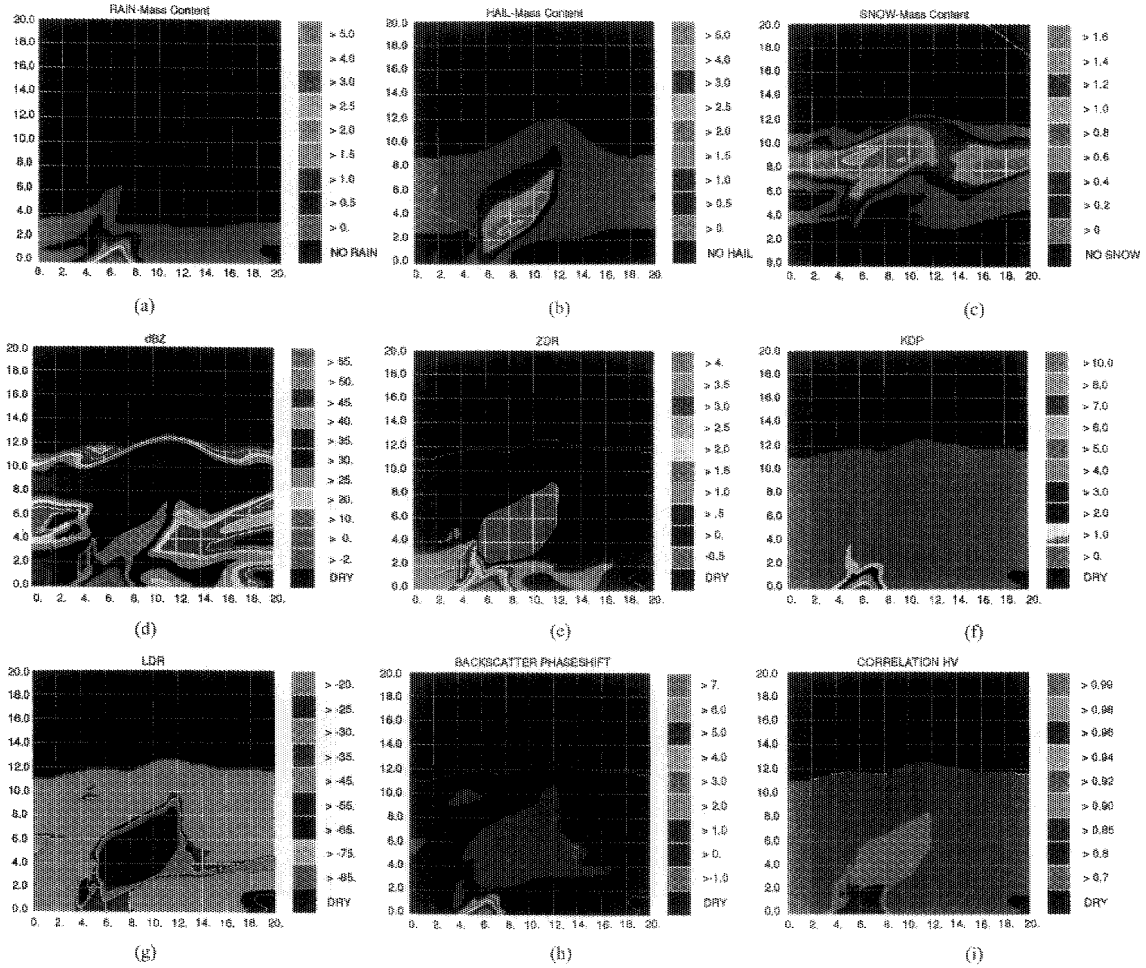

Fig. 11. Same as Fig. 9, except at time step 300.

C. Time Step 300 in the Simulation

Figs. 11(a)–(c) show contours of mass contents M_r, M_h, and M_s, respectively. The peak values of the mass contents for each category has reduced at this time step. A weaker updraft is still evident in the profile of M_r, with a peak value of M_r = 4.79 $g\ m^{-3}$ near the surface. M_h values in excess of 2.5 g\m^{-3} are seen just below the melting level, with small concentrations of hail and graupel near the surface. Figs. 11(d)-(i) show contours of the radar observables. Z_H values exceed 50 dBZ with a peak value $\sim$ 56 dBZ near the surface. The high values of Z_H combined with the high Z_{DR} values (greater than 3.5 dB in Fig. 11(e)) and the low ρ_{HV} values ($\approx$ 0.96 in Fig. 11(i)) indicate rain mixed with large hailstones and graupel at the surface. This is also evident from the high values of δ in Fig. 11(h), (greater than 6°) near the surface. The negative δ values above the melting level indicate the presence of larger ice particles. The positive column of Z_{DR} combined with the profile of K_{DP} (in Fig. 11(g)) indicate that the raindrops are still being carried aloft by the updraft that extends to the melting level. LDR values are quite similar to those seen at the previous time step. Attenuation values are lower than the previous time step with values $\sim$ 0.3 dB km^{-1} near the surface.

From the above discussions it is interesting to note that the ambiguities that might result in characterizing mixed phase precipitation using only Z_H, or Z_H and Z_{DR} are reduced by using additional measurements like K_{DP}, LDR, ρ_{HV} and δ.

VI. Conclusions

In this paper we have considered the effects of a mixture of precipitation particles on polarimetric radar parameters. The treatment is rigorous and considers the effects of particle size, shape, orientation and dielectric constant for each of the different species in the mixture. The scattering calculation is performed for oblate and conical shapes using the T-matrix method at both S and C-bands. The orientation probability distribution is two-dimensional in θ and ϕ. The $\phi-$distribution is assumed to be uniform in $[0, 2\pi]$ while the $\theta-$distribution is Gaussian $(\bar{\theta}, \sigma)$. By varying $\bar{\theta}$ and σ for the different species, such as raindrops, hail, graupel, ice crystals, and snow, it

is possible to simulate a variety of fall mode characteristics, the extremes being preferred alignment and complete random orientation. From the averaged Mueller matrix, a number of polarimetric radar parameters such as Z_{DR}, LDR, K_{DP}, ρ_{HV} and δ are calculated. These radar parameters have recently been shown to be linked to important microphysical properties. They are also measurable by coherent radars which possess dual-polarized capabilities [1].

The first part of the paper describes in detail the single particle radar parameters as a function of size assuming preferred orientation for the various precipitation types. The intent is to show both size dependence features such as Mie effects as well as dielectric constant dependence. We next show some results for simple two component mixtures such as rain/hail and ice crystals/snow. The independent variable is hail rate and snow reflectivity for the two cases. Suitable size distributions are assumed. These simple models clearly show how different species are responsible for the backscatter and forward-scatter properties. We also study the effects of varying elevation angles upon radar parameters. An important practical conclusion is that elevation angle corrections are unimportant if the elevation angle is less than 20°.

In order to consider realistic mixtures of precipitation types we have used results from a 2D numerical cloud model simulation of a convective storm. This model predicts the mass of rain, hail/graupel and snow in a 2D grid (vertical axis is height, horizontal axis is distance) at each time step which yields a series of vertical profiles of the mass of the three species. We have considered three phases of the storm, the initial, peak and dissipating stages separated by 15 min. Radar parameters calculated from the cloud model data show spatial and temporal evolution of the storm from a radar perspective. The polarimetric radar parameters also show the relationship between the different polarimetric parameters and the particle types/mass contents at different stages of the storm evolution. One important conclusion is that it is very difficult to detect snow using polarimetry because of its low density and tumbling motions. On the other hand, rain and graupel/hail are easily detected and quantified. Small scale features in the cloud model data such as strong vertical air currents transporting raindrops to higher altitudes are also visible in the radar parameters such as Z_{DR} and K_{DP}. The model results shown here will not only assist in the microphysical interpretation of radar measurements but also help in understanding the link between kinematical and radar-deduced microphysical fields.

ACKNOWLEDGMENT

Dr. F. Kopp of SDSM&T provided the numerical cloud model data. Computations were performed on the Cray-YMP at NCAR, Boulder, CO. Finally, the assistance of C. Makowski and D. Peters in preparing this manuscript is also gratefully acknowledged.

REFERENCES

[1] V. N. Bringi and A. Hendry, "Technology of polarization diversity radars for meteorology," in *Radar in Meteorology*, D. Atlas, Ed. Boston, MA: AMS, 1990, ch. 19a.

[2] M. P. M. Hall, W. F. Goddard, and S. M. Cherry, "Identification of hydrometeors and other targets by dual-polarization radar," *Radio Sci.*, vol. 19, pp. 132–140, 1984.

[3] A. R. Jameson, "Microphysical interpretation of multiparameter radar measurements in rain. Part III: Interpretation and measurements of propagation differential phase shift between orthogonal linear polarization," *J. Atmos. Sci.*, vol. 42, pp. 607–614, 1985.

[4] N. Balakrishnan and D. S. Zrnić, "Use of polarization to characterize precipitation and discriminate large hail," *J. Atmos. Sci.*, vol. 47, pp. 1525–1540, 1990.

[5] P. F. Meischner, V. N. Bringi, D. Heimann, and H. Hoeller, "A squall line in S. Germany: Kinematics and precipitation formation as deduced by advanced polarimetric and Doppler radar," *Mon. Weather Rev.*, vol. 119, no. 3, pp. 678–701, 1991.

[6] J. Hubbert, V. Chandrasekar, V. N. Bringi, and P. Meischner, "Processing and interpretation of coherent dual-polarized radar measurements," *J. Atmos. Ocean. Technol.*, 1992.

[7] D. S. Zrnić, N. Balakrishnan, C. L. Zeigler, V. N. Bringi and K. Aydin, "Polarimetric signatures in the stratiform region of a mesoscale convective system," *J. Appl. Meteor.*, in press, 1992.

[8] J. Vivekanandan, W. M. Adams, and V. N. Bringi, "Rigorous approach to polarimetric radar modeling of hydrometeor orientation distributions," *J. Appl. Meteorol.*, 30, pp. 1053–1063, 1991.

[9] P. Barber and C. Yeh, "Scattering of electromagnetic waves by arbitrarily shaped dielectric bodies," *Appl. Opt.*, vol. 14, pp. 2864–2872, 1975.

[10] D. Y. Wang, "Light scattering by nonspherical multilayered particles," doctoral thesis, Univ. of Utah, 1979.

[11] D. Husson and Y. Pointin, "Quantitative estimation of the hailfall intensity with a dual-polarization radar and a hailpad network," in*Preprints 24th Conf. Radar Meteorol.*, Tallahassee, 1989, pp 318–321.

[12] K. Aydin, Y. Zhao, and T. A. Seliga, "A differential reflectivity radar hail measurement technique: Observations during the Denver hail storm of 13 June 1984," *J. Atmos. Ocean. Technol.*, vol. 7, pp. 104–113, 1990.

[13] D. R. Longtin, C. F. Bohren, and L. J. Battan, " Radar backscattering by large, spongy ice oblate spheroids," *J. Atmos. Ocean. Technol.*, vol. 3, pp. 355–358, 1987.

[14] A. W. Green, " An approximation for shape of large raindrops," *J. Appl. Meteorol.*, vol 14, pp. 1578–1583, 1975.

[15] K. Aydin and V. Giridhar," C-band dual-polarization radar observables in rain," *J. Atmos. Ocean. Technol.*, vol. 9, pp. 383–390, 1992.

[16] T. A. Seliga and V. N. Bringi, "Differential reflectivity and differential phaseshift: Applications in radar meteorology," *Radio Sci.*, vol. 13, no. 2, pp. 271–275, 1978.

[17] K. Aydin, T. A. Seliga, and V. N. Bringi, "Differential radar scattering properties of hail and mixed phase hydrometeors," *Radio Sci.*, vol. 19, no. 1, 1984.

[18] M. J. Bader, S. A. Clough, and G. P. Cox, "Aircraft and dual-polarization radar observations of hydrometeors in light stratiform precipitation," *Quart. J. Roy. Meteorol. Soc.*, vol. 115, pp. 491–515, 1987.

[19] H. Uyeda, R. Shirooka, K. Iwanami, A. Takemoto, and K. Kikuchi, "Observations of vertical structures of convective snow clouds with a dual-polarized radar in Hokkaido, Japan," in *Proc. 25th Int. Conf. Radar Meteorol.*, Paris, 1991, pp. 717- 720.

[20] P. Meischner, M. Hagen, and V. N. Bringi, "Microphysics of snow formation of an Alpine upslope case," presented at the 11th Conf. Clds. Precip., Montreal, 1992.

[21] A. Hendry, G. C. McCormick, and B. L. Barge, "Ku-band and S-band observations of the differential propagation constant in snow," *IEEE Trans. Antennas Propagat.*, vol. AP-24, pp. 521–525, 1976.

[22] V. N. Bringi, T. A. Seliga, and W. A. Cooper, "Analysis of aircraft hydrometeor spectra and differential reflectivity radar measurements during the Cooperative Convective Precipitation Experiment," *Radio Sci.*, vol. 19, no. 1 , 1984.

[23] J. S. Marshall and W. McK. Palmer, "The distribution of raindrop size," *J. Appl. Meteorol.*, vol. 5, pp. 165–166, 1948.

[24] N. C. Knight, "Hailstone shape factor and its relation to radar interpretation of hail," *J. Climate Appl. Meteorol.*, vol. 25, pp. 1956–1958, 1986.

[25] L. Cheng and M. English, "A relationship between hailstone concentration and size," *J. Atmos. Sci.*, vol. 40, pp. 204–213, 1983.

[26] E. Torlaschi, R. G. Humphries, and B. L. Barge, "Circular polarization for precipitation measurements," *Radio Sci.*, vol. 19, pp. 193–200, 1984.

[27] W. C. Ulbrich and D. Atlas, "Hail parameter relations. A comprehensive digest," *J. Appl. Meteorol.*, vol. 21, pp. 22–43, 1982.

[28] J. D. Tuttle, V. N. Bringi, H. Orville, and F. Kopp, "Multiparameter radar study of a microburst: Comparison with model results," *J. Atmos. Sci.*, vol. 46, no. 6, 1989.

[29] R. R. Rogers, *A Short Course in Cloud Physics*. Permagon, 232 pp.

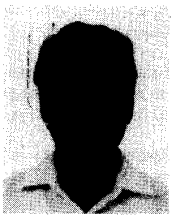

J. Vivekanandan received the B.E. degree in electronics and communications engineering from Maduraj-Kamaraj University, the M.Tech. degree in microwave and radar engineering from the Indian Institute of Technology, Kharagpur, India, and the Ph.D. degree in electrical engineering in 1986 from Colorado State University, Fort Collins.

At present he is a scientist at he National Center for Atmospheric Research, Boulder, CO. His research experience includes microwave radar and radiometer/satellite remote sensing of the atmosphere, vegetation, and soil. Recently, he has spent considerable effort in modeling polarimetric radar and multifrequency radiometer observations of clouds and their interpretations.

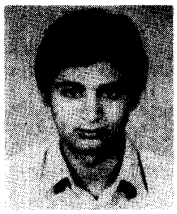

Ravikumar Raghavan (S'84–M'90) received the doctoral degree in electrical engineering from Colorado State University.

He is presently affiliated with the Institute for Global Change Research and Education at NASA/Marshall Space Flight Center. His research interests include radar/satellite remote sensing of the atmosphere and polarimetric radar techniques as applied to cloud physics and rainfall research. He is also involved in providing scientific support for the Lightning Imaging Sensor (LIS) research program at MSFC associated with TRMM.

V. N. Bringi was a member of the AMS Committee on Radar Meteorology. He is currently a member of the NEXRAD Technical Advisory Committee. His research interests over the last 15 years have been in the areas of electromagnetic wave propagation and scattering, multiple scattering of waves, polarimetric radar techniques, and applications to meteorology,

Dr. Bringi has received the following honors and awards: UCAR Fellowship (1974–1976), the Alumni Award for Graduate Student Research (1977) from Ohio State University, Colorado State University College of Engineering's Young Faculty Professional Development Award (1983), the Halliburton Young Faculty Research Award (1984), and the Dean's Council Award (1989).